

# Atomic clock locking via Bayesian frequency estimation

Chengyin Han,<sup>1</sup> Zhu Ma,<sup>2,1</sup> Yuxiang Qiu,<sup>2,3</sup> Ruihuan Fang,<sup>2,1</sup> Jiatao Wu,<sup>2,1</sup> Chang Zhan,<sup>2,1</sup> Maojie Li,<sup>2,1</sup> Jiahao Huang,<sup>1,2,\*</sup> Bo Lu,<sup>1,†</sup> and Chaohong Lee<sup>1,4,‡</sup>

<sup>1</sup>*Institute of Quantum Precision Measurement, State Key Laboratory of Radio Frequency Heterogeneous Integration, College of Physics and Optoelectronic Engineering, Shenzhen University, Shenzhen 518060, China*

<sup>2</sup>*Laboratory of Quantum Engineering and Quantum Metrology, School of Physics and Astronomy, Sun Yat-Sen University (Zhuhai Campus), Zhuhai 519082, China*

<sup>3</sup>*College of Physics and Electronic Science, Hubei Normal University, Huangshi 435002, China*

<sup>4</sup>*Quantum Science Center of Guangdong-Hong Kong-Macao Greater Bay Area (Guangdong), Shenzhen 518045, China*

(Dated: March 13, 2024)

Atomic clocks play a vital role in fundamental science and practical technology. However, their sensitivity is typically limited by the standard quantum limit, which is determined by parallel measurements with individual particles or repeated measurements with a single particle. Overcoming this limitation requires exploiting correlations between particles or interrogation times. While it has been demonstrated that sensitivity can be improved to the Heisenberg limit by utilizing quantum entanglement, it remains unclear whether the scaling of sensitivity with respect to total interrogation time can achieve the Heisenberg scaling. Here, we develop an adaptive Bayesian frequency estimation protocol that approaches the Heisenberg scaling and experimentally demonstrate its validity with a cold-atom coherent-population-trapping clock. In further, we achieve robust closed-loop locking of the atomic clock by utilizing our Bayesian frequency estimation protocol. In comparison with the conventional clock locking, our Bayesian clock locking yields an improvement of 5.1(4) dB in fractional frequency stability. Our findings not only provide an alternative approach to locking atomic clocks but also hold promising applications in other quantum sensors, such as quantum magnetometers and atomic interferometers.

Atomic clocks operate by precisely detecting the transition frequency between two specific atomic levels while simultaneously synchronizing this transition with a local oscillator (LO) [1]. These state-of-the-art atomic clocks have broad applications in time-keeping, global positioning systems, telecommunications, and also contribute to the search for new physics [2–6]. The measurement noise in atomic clocks is typically dominated by quantum projection noise (QPN). The sensitivity of the frequency measurement in atomic clocks utilizing repeated identical Ramsey interferometry is commonly described by  $\Delta f_{est}(N, T) \propto (N \cdot T \cdot T_s)^{-1/2}$ . Here  $N$  is the total particle number,  $T$  is the total interrogation time, and  $T_s$  is the interrogation time for each Ramsey interferometry. This means that the sensitivity obeys the standard quantum limit (SQL) ( $\Delta f_{est} \propto N^{-1/2}$ ) with respect to the total particle number  $N$  and the SQL ( $\Delta f_{est} \propto T^{-1/2}$ ) with respect to the total interrogation time  $T$ .

Utilizing correlations between particles or interrogation times can effectively enhance sensitivity. Quantum entanglement has been extensively employed to improve sensitivity from SQL to sub-SQL scaling ( $\propto N^{-\alpha}$  with  $0.5 < \alpha \leq 1$ ) [7–17]. However, for metrological applications, it is necessary to directly observe stability enhancement without the post-processed removal of technical noise [7, 9, 15]. Alternatively, sensitivity can be improved by utilizing the correlation between measurements with different interrogation times. In addition to conventional frequentist estimation, well-designed Bayesian estimation protocols with different interrogation times can improve sensitivity to sub-SQL scaling ( $\propto T^{-\alpha}$ ) [18] or even achieve Heisenberg scaling ( $\alpha = 1$ ) [19–21]. These ap-

proaches have been successfully applied to improve magnetometers [22–26], but the utilization of Bayesian estimation protocols to enhance atomic clocks has not been reported.

In addition to sensitivity, stability is another crucial factor that characterizes the performance of atomic clocks [1, 27]. Generally, the QPN-limited fractional stability is directly proportional to the sensitivity [28] for a given total interrogation time  $T$ . Therefore, by employing Bayesian frequency estimation to enhance sensitivity within the allotted interrogation time  $T$ , it becomes possible to improve the stability of an atomic clock. Furthermore, the Bayesian estimation protocol naturally provides frequency feedback, making it highly suitable for high-stability atomic clock locking. By employing Bayesian estimation, we can reduce the overall measurement time required to lock an atomic clock and enhance robustness against technical noises, leading to improved stability.

In this article, we develop and experimentally demonstrate a Bayesian frequency estimation (BFE) protocol using an ensemble of laser-cooled  $^{87}\text{Rb}$  atoms in coherent population trapping (CPT). We utilize this protocol to achieve robust closed-loop locking of a cold-atom CPT clock. The BFE protocol is specifically designed to measure the clock transition frequency of  $^{87}\text{Rb}$  through the exponential increase of interrogation time in CPT-Ramsey interferometry. It also adaptively adjusts the LO frequency during Bayesian updates. Our protocol exhibits a standard deviation that follows Heisenberg scaling ( $\Delta f_{est} \propto T^{-1}$ ), which surpasses the SQL scaling ( $\Delta f_{est} \propto T^{-1/2}$ ). Furthermore, we successfully lock a

cold-atom CPT clock using our BFE approach, resulting in a fractional frequency stability of  $4.3(2) \times 10^{-12}/\sqrt{\tau}$ . This represents an improvement of 5.1(4) dB compared to the fractional frequency stability  $1.4(1) \times 10^{-11}/\sqrt{\tau}$  obtained by the proportional-integral-differential (PID) locking method. If these findings are applied to many-body quantum systems, they could mitigate QPN with respect to both the particle number ( $N$ ) and the interrogation time ( $T$ ). This holds great promise for enhancing the sensitivity of practical quantum sensors.

## Experimental system

Instead of using a microwave cavity, CPT [29] interrogates the atomic transitions of alkali atoms optically. Therefore, CPT atomic clocks have an advantage of low power consumption and small size, which is suitable for developing chip-scale atomic clocks [30–32]. The experimental setup of cold-atom CPT system is similar to our previous work [33, 34] and is shown in Fig. 1. The details can be seen in the Methods. We utilize a single- $\Lambda$  CPT scheme (Fig. 1a) to avoid time-dependent intervening between multi-path CPT in the lin||lin or lin $\perp$ lin scheme [35–39]. In a CPT-Ramsey interferometry, the probability amplitude of the excited state undergoing is given by  $P_e = \alpha e^{-\alpha\Gamma\tau_d} [1 - (1 - e^{-\alpha\Gamma\tau_p}) |\sec(\alpha)| \times \cos(f - f_c + f_s) T_R]$ , where  $\alpha = \Omega^2/(\Gamma^2 + 3\Omega^2 + 4\delta^2)$  represents the interaction with the CPT pulse,  $T_R$  is the Ramsey time,  $\Omega$  is the average Rabi frequency,  $\delta$  is the single-photon detuning,  $\tau_p$  and  $\tau_d$  are CPT preparation pulse duration and CPT detection pulse duration,  $f_c$  is the clock transition frequency,  $f_s$  is the  $T_R$ -dependent frequency shift and  $\Gamma$  is the decay rate of the excited state. In our experiment, only the LO frequency  $f$  and the Ramsey time  $T_R$  are tunable, thus the transmission signal becomes proportional to the cosine term, i.e.,  $S_{TS} \propto \cos(f - f_c + f_s) T_R$ .

## Bayesian frequency estimation

Unlike the frequentist estimation, the Bayesian estimation relies on updating the current knowledge of parameters after each experiment by means of Bayes' law [40]. It is particularly suitable for adaptive experiments in which measurement can be optimized based on the current knowledge of parameters. The adaptivity can improve sensitivity and save time compared with the frequentist estimation. It has been demonstrated that the sensitivity of Ramsey interferometry via single spin systems can surpass the SQL [21, 22, 24, 25, 41]. However, single spin systems can only provide a binary data in each measurement and the efficiency is easily affected by quantum shot noise and decoherence. Quantum sensors with atomic ensembles have the advantages of larger particle number  $N$  and higher signal-to-noise ratio (SNR). Below we present how the Bayesian estimation can be used to improve the frequency measurement precision and the stability of atomic clocks based upon ensembles.

In the Bayesian frequency estimation based upon

Ramsey interferometry, the normalization of the CPT-Ramsey signal  $S_{TS}$  can be expressed as

$$s_f = \frac{1}{2} [1 + \cos 2\pi(f - f_c + f_s) T_R]. \quad (1)$$

The normalization is feasible as long as more than a period of oscillation can be achieved. In a single-particle Ramsey interferometry, the likelihood function reads  $\mathcal{L}_u(u|f_c, f) = \frac{1}{2} [1 + (-1)^u \cos 2\pi(f - f_c + f_s) T_R]$ , where  $u = 0$  or  $1$  stand for the particle occupying the clock state  $|F = 1, m_F = 0\rangle$  or  $|F = 2, m_F = 0\rangle$  respectively. In the CPT-Ramsey interferometry, the signal of each measurement is provided by an ensemble of atoms rather than a single atom. This implies that the probability ( $p_e$ ) of the atoms occupying the clock state follows a binomial distribution, which can be approximated by a Gaussian distribution when the total particle number in the experiment is sufficiently large. Thus we use a Gaussian distribution function as our likelihood function [42],

$$\mathcal{L}(p_e|f_c, f) = \frac{1}{\sqrt{2\pi}\sigma} \exp \left[ -\frac{(p_e - \mathcal{L}_u(1|f_c, f))^2}{2\sigma^2} \right], \quad (2)$$

where  $\sigma^2 \approx p_e(1-p_e)/R = s_f(1-s_f)/R$  with  $s_f$  the normalized Ramsey signal and  $R$  determined by the signal's SNR ( $R = 1540$  for our experiment, see Supplementary Materials). This likelihood  $\mathcal{L}(p_e|f_c, f)$  is a function of  $p_e$  with respect to  $f$ . In the Bayesian update, the probability distribution is updated according to the Bayes' formula,

$$p_i(f_c|p_e; f) = \mathcal{N} \mathcal{L}(p_e|f_c, f) p_{i-1}(f_c), \quad (3)$$

where  $\mathcal{N}$  is a normalization factor and the initial prior function  $p_1(f_c)$  can be chosen as a uniform distribution function over the measurement range of  $f_c$  (See Algorithm 1 in Method). In the  $i$ -th update, we obtain a posterior function  $p_i(f_c|p_e; f)$ , and the estimator of  $f_c$  can be given as  $f_{\text{est}}^{(i)} = \int f_c p_i(f_c|p_e; f) df_c$  with a standard deviation  $\Delta f_{\text{est}}^{(i)} = \sqrt{\int f_c^2 p_i(f_c|p_e; f) df_c - (f_{\text{est}}^{(i)})^2}$ . The next update is implemented by inheriting the posterior function as the next prior function  $p_{i+1}(f_c) = p_i(f_c|p_e; f)$ .

For the periodic probability distribution Eq. (1) and the Gaussian likelihood Eq. (2), one may use the adaptive strategy with exponentially sparse interrogation times [18, 24, 25, 41, 43, 44]. To estimate the clock frequency, we adaptively adjust the LO frequency according to the posterior distribution during Bayesian updates. The procedure of BFE protocol is sketched in Fig. 2a. At begin, the interrogation time  $T_1$  and the LO frequency  $f$  should be preset. Here, we denote the interrogation time in the  $i$ -th Bayesian update as  $T_R^{(i)} \equiv T_i$ . In practice,  $T_i$  is limited by the coherence time  $T_{\text{max}}$ .

To design an optimal exponentially increasing time sequence, we set the last interrogation time  $T_{M_b} = T_{\text{max}}$  and derive the previous interrogation times as

$$T_i = T_{\text{max}} / a^{M_b - i} \quad (4)$$

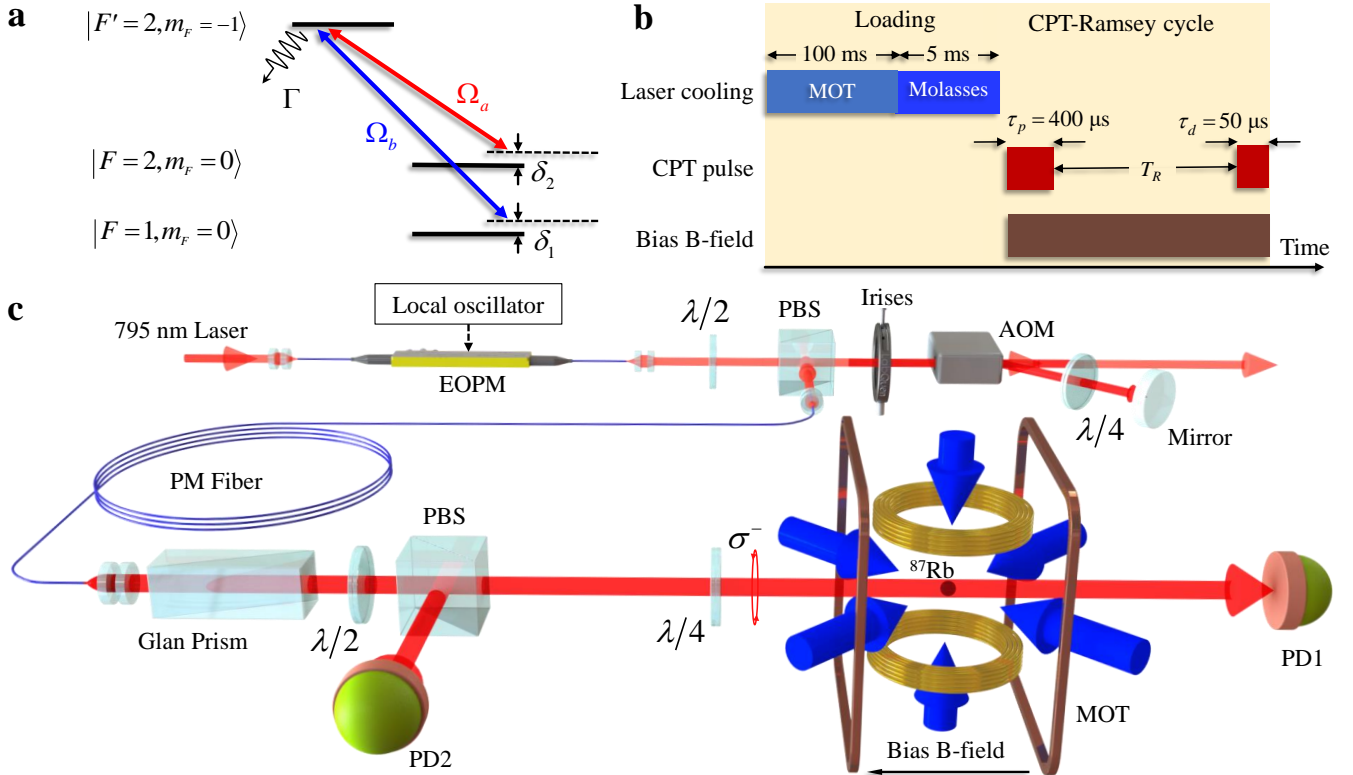


FIG. 1. **Experimental setup.** **a**, A typical three-level A system in  $^{87}\text{Rb}$ . In our experiment, the two clock states ( $|F=1, m_F=0\rangle$  and  $|F=2, m_F=0\rangle$ ) are coupled through the excited state  $|F'=2, m_F=-1\rangle$ . **b**, The timing sequence for an experimental cycle. The loading process contains 100 ms MOT and 5 ms molasses. The CPT-Ramsey process includes a 400  $\mu\text{s}$  preparation pulse  $\tau_p$ , a Ramsey time  $T_R$  and a 50  $\mu\text{s}$  detection pulse  $\tau_d$ . The bias magnetic field aligned with the CPT laser beam is applied in the CPT-Ramsey process to split the Zeeman sublevels. **c**, Experimental setup. The CPT beam is generated and modified by a fiber-coupled EOPM, an AOM and a Glan prism. To increase signal robustness to laser intensity noise, the CPT beam is separated into a transmission beam and a reference beam by a half-wave plate and a PBS. The  $\sigma-\sigma$  configuration of the CPT beam is realized by a quarter-wave plate according to the bias B-field. AOM: acousto-optic modulator, EOPM: electro-optic phase modulator, GP: Glan prism, PBS: polarization beam splitter, PD: photodetector,  $\lambda/2$ : half-wave plate,  $\lambda/4$ : quarter-wave plate.

with  $a > 1$ . The number of iterations  $M_b = \log_a(T_{\max}/T_{\min}) + 1$  can be determined by the ratio between maximum and minimum interrogation times. The interrogation time  $T_i$  in our experiment is limited up to  $T_{\max} = 20$  ms due to the freely falling atoms will be out of the CPT beam if  $T_i > T_{\max}$ . The available  $T_{\min}$  in our experiment is  $T_1 = T_{\min} \geq 0.2$  ms. Thus, the total interrogation time is  $T = \sum_{i=1}^{M_b} T_i \approx T_{\max} \frac{a}{a-1}$ . The initial probability distribution of  $f_c$  is set in the interval  $[f_l, f_r]$  of width  $f_{lr} \equiv f_r - f_l = 1/T_1$ . In the iteration, after each update via Eq. (3), the corresponding frequency range interval is turned into  $[f_{\text{est}}^{(i)} - 1/2T_i, f_{\text{est}}^{(i)} + 1/2T_i]$  as  $T_i$  increases.

In the adaptive procedure (see Fig. 2a), the LO frequency  $f_i$  for the  $i$ -th update is adaptively determined based on the previous posterior function  $p_{i-1}(f_c|p_e; f)$ . In this way the likelihood function (2) is updated adaptively so that the spurious peaks in the posterior functions can be eliminated [45]. To determine the value of  $f_i$ , we use the expected gain in Shannon information of

the posterior function [46]. Different from the summation over many single-shot measurements [46], we measure an ensemble of particles and the corresponding Utilize function becomes

$$U_f = \int_0^1 dp_e \int U_{p_e, f} \mathcal{L}(p_e|f_c, f) p(f_c) df_c, \quad (5)$$

where

$$U_{p_e, f} = \int p(f_c|p_e; f) \ln [p(f_c|p_e; f)] df_c - \int p(f_c) \ln [p(f_c)] df_c \quad (6)$$

is the expected gain in Shannon information of the posterior function with respect to the prior function. Thus the LO frequency  $f_i$  is chosen as the one that maximizing  $U_{f_i}$ . In a realistic experiment, we calculate the Utilize function by discretizing the integral over  $p_e$ , see details in Supplementary Materials.

Once  $f_i$  and  $T_i$  are given, a measurement can be made to obtain a normalized signal  $s_{f_i}$ . Due to the

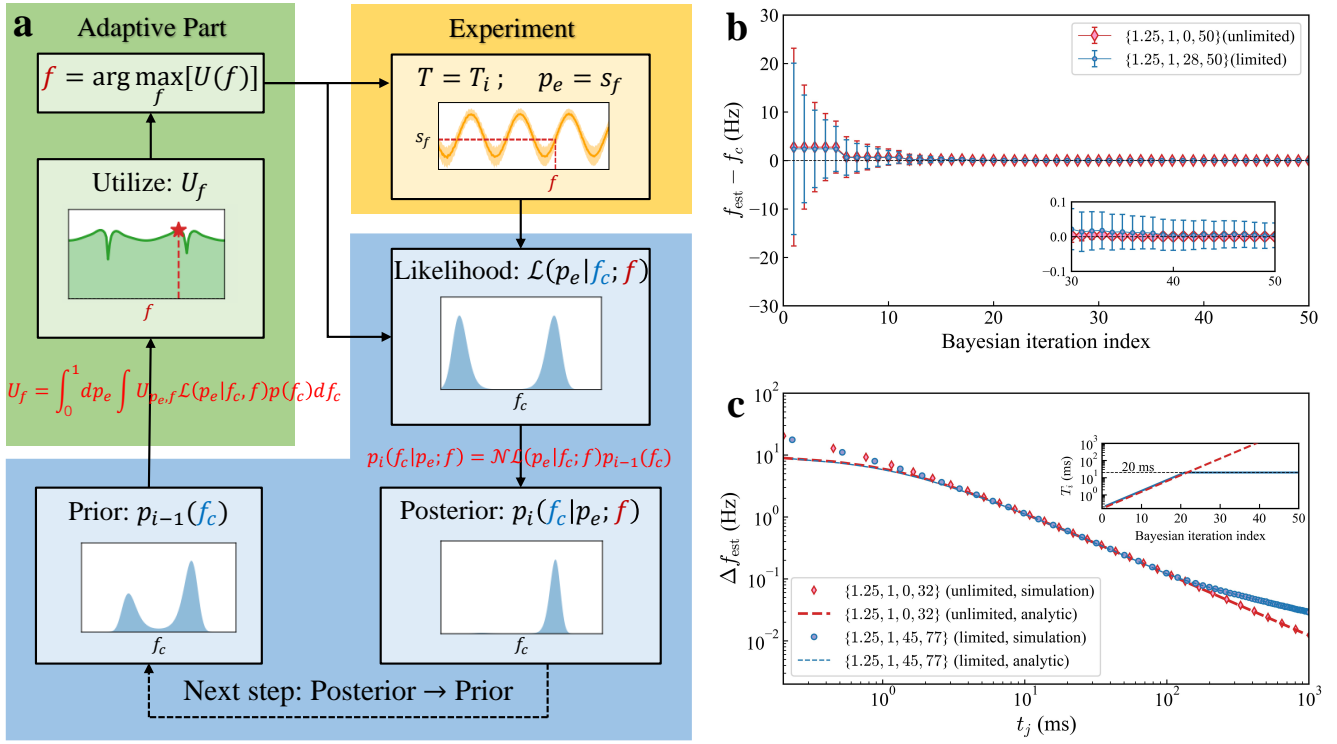


FIG. 2. **Schematic and performance of our Bayesian frequency estimation (BFE) protocol.** **a**, Schematic of our BFE protocol. Given a prior function  $p_{i-1}$  obtained in the previous update, a likelihood function is accordingly obtained and the posterior function is updated through the Bayes' formula Eq. (3). The likelihood function is obtained with the LO frequency  $f$  optimized by the Utilize function Eq. (5). **b**, The difference between the estimated and exact frequencies rapidly converges to zero. Red line: the case of increasing individual interrogation times  $T_i$  without limitation  $\{a = 1.25, g = 1, \tilde{M} = 0, M_b = 50\}$ . Blue line: the case of increasing individual interrogation times  $T_i$  under limitation  $T_i \leq T_{max}$   $\{a = 1.25, g = 1, \tilde{M} = 28, M_b = 50\}$ . The errorbars denote the standard deviations. **c**, The standard deviation versus the interrogation time  $t_j = \sum_{i=1}^j T_i$  for limitation  $\{a = 1.25, g = 1, \tilde{M} = 45, M_b = 77\}$  and unlimitation  $\{a = 1.25, g = 1, \tilde{M} = 0, M_b = 32\}$  while  $t_j$  is up to 1000 ms. Inset: the individual interrogation time  $T_i$  versus the number of Bayesian iteration index with and without limitation.

$T_i$ -dependent frequency shift  $f_s$  in the CPT-Ramsey interferometry, a measurement of  $f_s$  prior to the update should be made for a compensation (see details in Supplementary Materials). In Fig. 2, we show the performance of BFE algorithm through numerical simulation. By setting  $a = 1.25$ , the estimated value  $f_{est}$  is gradually converged to the clock transition frequency  $f_c$  as iterations increase. The scaling of the standard deviation

$$\Delta f_{est} \approx \sqrt{1 + \frac{2}{a-1}} \frac{1}{2\pi\sqrt{RT}} \quad (7)$$

versus the total interrogation time  $T = \sum_{i=1}^{M_b} T_i$  [19] obeys the Heisenberg scaling  $\Delta f_{est} \propto T^{-1}$ .

In a conventional frequentist estimation of  $T/T_s$  times of independent measurements over a fixed interrogation time  $T_s$ , which always satisfies  $T_s \ll T$ , the standard deviation obeys the SQL scaling  $\propto 1/\sqrt{TT_s} \propto 1/\sqrt{T}$ . It should emphasize that for the special case where only one measurement is performed with  $T = T_s$ , the standard deviation would be  $\propto 1/\sqrt{TT_s} \propto 1/T$ . However, this scaling will not hold when  $T > T_s$ . In contrast, in our

Bayesian estimation procedure, we perform a sequence of correlated measurements with increasing interrogation times  $T_i$  over the whole duration  $T = \sum_{i=1}^{M_b} T_i$ , in which the parameters for the next measurement are determined by its previous measurements. Therefore the standard deviation of our Bayesian estimation procedure attains the Heisenberg scaling  $\propto 1/T$  during  $T$  (see Supplementary Materials). Since the scaling is inversely proportional to the total interrogation time  $T = aT_{max}/(a-1)$  rather than a single Ramsey interrogation time  $T_s$ , the scaling  $\propto 1/T$  can hold for  $T \gg T_s$ . This scaling is very different from the sensitivity scaling obtained by conventional frequentist estimation, which is just the SQL.

In comparison with the conventional frequentist estimation, our BFE exhibits high dynamic range. For the conventional frequentist estimation, one may choose  $T_s = T_{max}$  to achieve the highest precision measurement, but the corresponding dynamic range would become small due to the phase ambiguities [18, 24, 43]. However, for our BFE, its dynamic range is determined by the minimum interrogation time  $T_1$  in the measurement sequence and its measurement precision can be im-

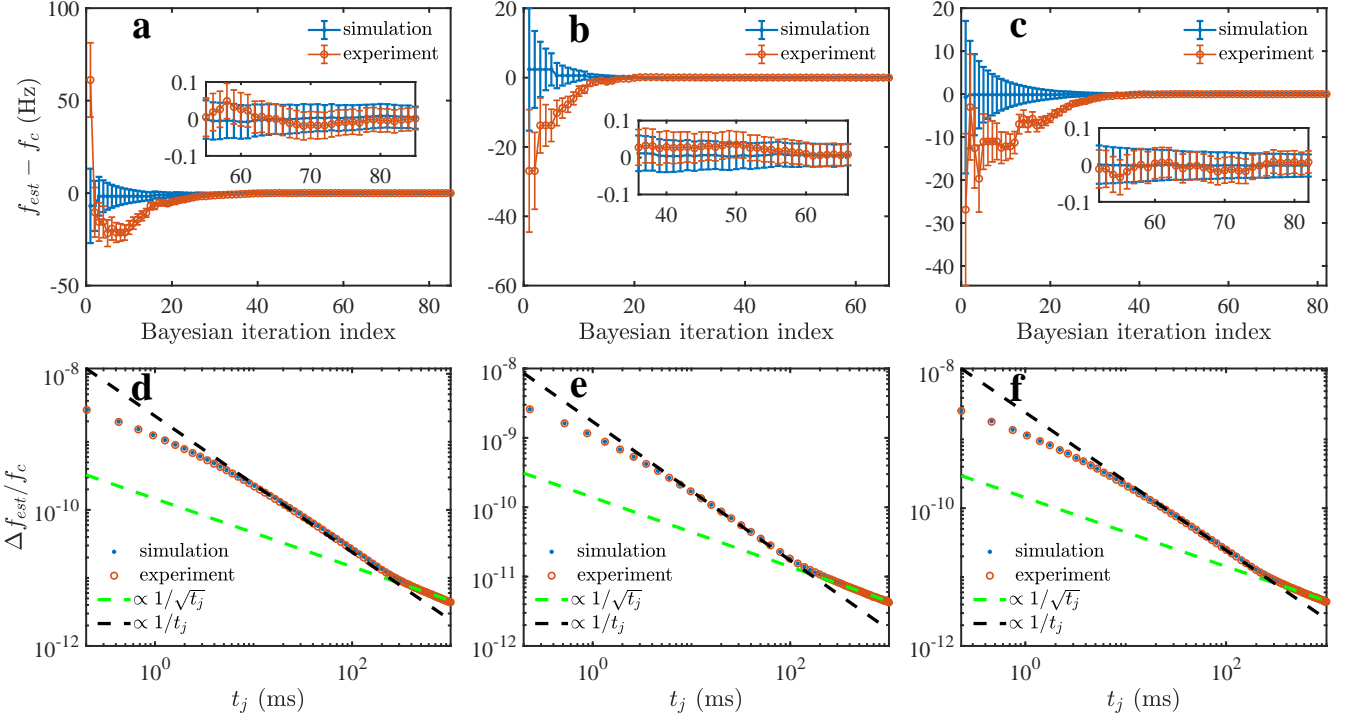


FIG. 3. **Experimental demonstration of Bayesian frequency estimation.** The results from the experiment for  $\{a = 10/9, g = 1, \tilde{M} = 40, M_b = 85\}$  is shown in **a** and **d**, while the results for  $\{a = 1.25, g = 1, \tilde{M} = 44, M_b = 66\}$  and  $\{a = 1.25, g = 2, \tilde{M} = 37, M_b = 81\}$  are shown in **b** and **e**, and **c** and **f** respectively. The estimated frequency difference versus the Bayesian iteration index are plotted on the top including the corresponding standard deviations shown as errorbars, while the standard deviations versus the interrogation time  $t_j = \sum_{i=1}^j T_i$  are shown on bottom. We also provide numerical and analytic results for comparison. In **a**, **b** and **c** the estimated values and the standard deviation decrease rapidly and we zoom in the last 30 results in the insets.

proved without sacrificing the dynamic range (see Supplementary Materials). Besides, our BFE has much better robustness against experimental technical noises (see Supplementary Materials).

Given a total interrogation time  $T$ , there are various routines to improve measurement precision by employing Bayesian update. First, choose the last interrogation time as  $T_{max}$  and change  $T_i$  every  $g$  steps, that is,  $T_{M_b} = T_{max}$  and  $T_i = T_{max}/a^{\lceil(M_b-i)/g\rceil}$  with  $a = T/(T - gT_{max})$  and  $g$  being a positive integer. Thus we have the total iteration number  $M_b = g[\log_a(T_{max}/T_{min}) + 1]$  and the final measurement precision  $\Delta f_{est}^{(M_b)} \approx \sqrt{1 - \frac{1}{a^2} \frac{1}{2\pi\sqrt{g\sqrt{RT_{max}}}}}$  (see Supplementary Materials). When  $g = 1$ , it simplifies to a monotonically exponential increase as shown in Eq. (4). Second, choose  $T_j = T_{max}$ ,  $T_i = a^{i-1}T_1$  if  $i < j$ , and  $T_i = T_{max}$  if  $i \geq j$ . In this scenario, the value of  $T_i$  increases exponentially from  $T_1$  to  $T_{max}$  within the first  $j$  steps, and subsequently  $T_i$  stays constant at  $T_{max}$  for the remaining  $\tilde{M} = (M_b - j)$  steps. Therefore we have the total iteration number  $M_b = \{[T - aT_{max}/(a - 1)]/T_{max} + \log_a(T_{max}/T_{min}) + 1\}$  and the final measurement precision  $\Delta f_{est}^{(M_b)} \approx$

$\sqrt{\frac{1}{\tilde{M} + \frac{a^2}{a^2 - 1}} \frac{1}{2\pi\sqrt{RT_{max}}}}$  with  $a = \frac{T - \tilde{M}T_{max}}{T - (\tilde{M} + 1)T_{max}}$  (see Supplementary Materials), as shown in Fig. 2c. Third, combining the previous two schemes, choose  $T_j = T_{max}$ ,  $T_i = T_{max}/a^{\lceil(j-i)/g\rceil}$  if  $i < j$  (where  $j$  is a multiple of the positive integer  $g$ ), and  $T_i = T_{max}$  if  $i \geq j$ . For convenience, we label the above three schemes with  $\{a, g, \tilde{M}, M_b\}$ .

We use the BFE protocol to measure the clock transition frequency of  $^{87}\text{Rb}$  atom via CPT in a cold atomic ensemble. The experiment is performed automatically with the help of a computer connecting with digital I/O devices. The BFE protocol used in our experiment is executed individually to the numerical simulation, except the parameter  $p_e$  that is dependent on the normalized Ramsey signals  $s_f$ . By choosing  $T_1 = 0.2$  ms, without loss of generality, we set the frequency range  $[f_l = f_c - 3 \text{ kHz}, f_r = f_c + 2 \text{ kHz}]$  as the initial interval. As  $T_1$  and  $a$  are preset, we can compensate the  $T_i$ -dependent frequency shift  $f_s$  via adding it to the LO frequency as  $f'_i = f_i + f_s$ . Then two varying parameters  $T_i$  and  $f'_i$  in each update can be obtained via Eqs. (4) and (5), respectively. These two parameters are sent to the digital I/O devices that control a FPGA to generate a CPT-Ramsey sequence and scan the LO frequency

to acquire the CPT-Ramsey fringe. The normalized signal  $s_{f_i}$  is extracted by cosine fitting of the CPT-Ramsey fringe. The LO is referenced to a high-performance rubidium atomic clock with stability of  $6 \times 10^{-13}$  at 1 s.

In Fig. 3, we show the experimental demonstration of our BFE protocol. In our experiment, the maximum interrogation time is set as  $T_{max} = 20$  ms. The measurements of the clock transition frequency  $f_c$  are implemented with three different Bayesian update schemes:  $\{a = 10/9, g = 1, \tilde{M} = 40, M_b = 85\}$ ,  $\{a = 1.25, g = 1, \tilde{M} = 44, M_b = 66\}$  and  $\{a = 1.25, g = 2, \tilde{M} = 37, M_b = 81\}$ . When the iteration number is small, the estimated value  $f_{est}$  from the experiments deviate from numerical and analytic results due to the influence of experimental noises (see Fig. 3a, Fig. 3b and Fig. 3c). However, it gradually converges to an acceptable value within  $1\sigma$  standard deviation as the Bayesian iteration number increases. Meanwhile the standard deviations provided by the BFE protocol agree well with the numerical and analytic ones, as shown in Fig. 3d, Fig. 3e and Fig. 3f. Notably, the fractional measurement precision  $\Delta f_{est}/f_c$  follows the Heisenberg scaling before  $T_i$  reaches  $T_{max}$ .

### Closed-loop locking of the cold-atom CPT clock

In a conventional closed-loop locking of an atomic clock, the clock transition frequency is acquired by the alternate measurements of the transition probability at bilateral half-maximum points of atomic resonance line. The corresponding error signal is derived from the transition probability difference and fed back to stabilize the LO frequency by a PID controller, as shown in Fig. 4a. We use a CPT-Ramsey fringe with the Ramsey time  $T_R = 20$  ms to closed-loop lock the cold-atom CPT clock. The error signal  $\Delta\nu$  is calculated from  $f_c^j = \frac{S_{TS}(f_c^{j-1} + 1/4T_R) - S_{TS}(f_c^{j-1} - 1/4T_R)}{4T_R P}$ , where  $f_c^j$  is the clock transition frequency after the  $j$ -th feedback cycle and  $P$  is the amplitude of  $S_{TS}$ . The frequency fluctuation  $\delta\nu_j = f_c^j - f_c$  and the corresponding Allan deviations are shown in Fig. 4c and Fig. 4e (in red colour).

Using the developed BFE protocol, we stabilize the LO frequency to the atomic reference and realize robust closed-loop locking of a cold-atom CPT clock. The BFE procedure is carried out to acquire the clock transition frequency and directly feed back to the LO frequency via the error signal  $\Delta\nu_j = f_{est}^j - f_{est}^{j-1}$ . Here  $f_{est}^j$  is the  $j$ -th estimated value of clock transition frequency obtained by  $M_b$  Bayesian updates, see Fig. 4b. This means that we need  $M_b$  measurements of  $s_{f_i}$  to achieve one feedback rather than two measurements of  $S_{TS}$  for conventional locking. In the closed-loop locking of the cold-atom CPT clock, we choose the BFE scheme of parameters  $\{a = 1.25, g = 1, \tilde{M} = 6, M_b = 13\}$ . By increasing  $T_i$  in every Bayesian update from the initial interrogation time  $T_1 = T_{max}/1.25^{M_b - \tilde{M} - 1}$  ms to the maximum interrogation time  $T_{max} = 20$  ms, we realize a robust locking of the cold-atom CPT clock. The total interrogation time  $T$  is about 199 ms, which is about 5 times longer than that of conventional locking. In Fig. 4d and Fig. 4e, we

show our experimental results (in black colour) obtained via the BFE locking. Notably, the frequency fluctuation  $\delta\nu_j = f_{est}^j - f_c$  of BFE locking is about 3 times smaller than that of conventional locking with a PID controller.

To assess the clock stability, we analyze the Allan deviations for different locking schemes. As the transmission signal  $S_{TS}$  detected in our experiment is proportional to the excited-state population rather than the clock-state population, the normalized signal  $s_f$  is used for BFE. In our experiment,  $s_f$  is obtained by scanning the CPT-Ramsey fringe, and so that we expend more time to measure  $s_{f_i}$  than  $S_{TS}$ . However, for ion trap clocks, fountain clocks and optical lattice clocks, the transition probability at LO frequency  $f_i$  could be directly probed by the electron shelving technique [1, 47, 48] and the corresponding measurement times will decrease greatly. Anyway, the clock cycle time (a feedback time)  $T_c$  contains the total interrogation time  $T$  and dead time  $T_d$ . Then the averaging time can be expressed as  $\tau = M_c T_c = M_c(T + T_d)$ , where  $M_c$  is the total feedback number. Here, we use a total interrogation time of a feedback cycle  $T = 199$  ms for BFE locking while  $T = 40$  ms is used for the conventional locking. Due to the indirect detection of  $s_f(f_i)$ , the dead time is different for the two locking methods. In our clock locking via BFE, the limitation of short-term stability by Dick effect is estimated as  $2.4 \times 10^{-12}/\sqrt{\tau}$  according to the sensitivity function [49] and the LO phase noises (see Supplementary Materials).

To facilitate the comparison of the two locking schemes without loss of generality, the dead time is ignored when we calculate the Allan deviation. The BFE locking yields a stability of  $4.3(2) \times 10^{-12}/\sqrt{\tau}$ , which is  $5.1(4)$  dB better than the stability  $1.4(1) \times 10^{-11}/\sqrt{\tau}$  obtained by the PID locking. By setting  $\tau$  as unit time, the fractional stability  $\sigma \propto \Delta f_{est}$ . Owing to the Heisenberg-scaling measurement of the clock transition frequency achieved by the designed BFE, our cold-atom CPT clocks via BFE locking has an enhancement of stability (see Supplementary Materials). Our BFE locking method could be directly extended to fountain clocks [48], ion trap clocks [50, 51] and optical lattice clocks [52–56], which would be easier to implement than the cold-atom CPT clock as their transition probability can be directly measured via probing the clock-state population.

### Discussions

In conclusion, by designing an adaptive BFE protocol, we experimentally demonstrate the Heisenberg-scaling measurement of the clock transition frequency with respect to the interrogation time and use it to lock a cold-atom CPT clock with a better stability. The BFE is carried out to measure  $^{87}\text{Rb}$  clock transition frequency via exponentially step-wise increasing the interrogation time of CPT-Ramsey interferometry and adaptively adjusting the LO frequency during Bayesian updates. The measurement sensitivity versus the interrogation time beats the standard quantum limit ( $\Delta f_{est} \propto 1/\sqrt{T}$ ) and reaches

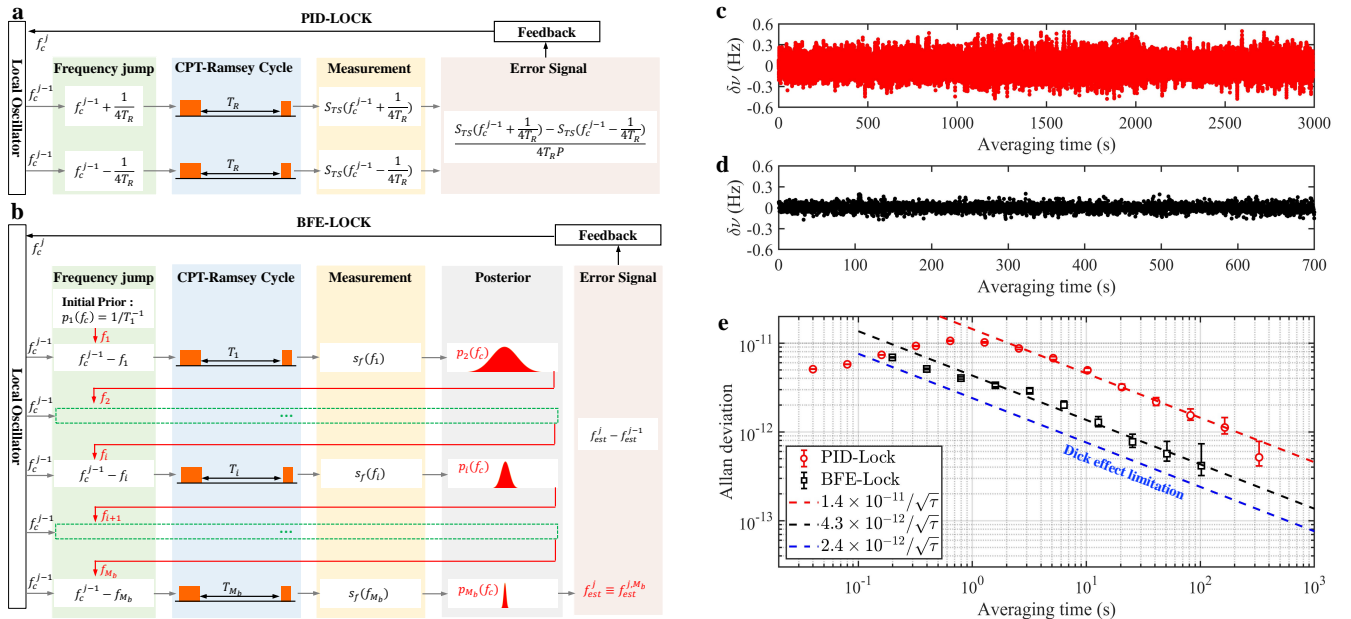


FIG. 4. **Closed-loop locking of a cold-atom CPT clock.** **a**, Locking a cold-atom CPT clock via conventional PID controller. Two measurements of  $S_{TS}$  at bilateral half-maximum points ( $f_c^{j-1} + 1/4T_R$  and  $f_c^{j-1} - 1/4T_R$ ) is used to derived the error signal and fed back to the LO. **b**, Locking a cold-atom CPT clock via Bayesian frequency estimation. 13 Bayesian iterations are used to estimate the clock transition frequency  $f_c$  and no feedback is provided to the LO until completion of all 13 Bayesian iterations. **c**, The frequency fluctuation for conventional closed-loop locking. **d**, The frequency fluctuation for BFE locking. **e**, Allan deviation of PID locking and BFE locking. The red dot and dashed line are the results from PID locking, while the black square and dashed line are the results from BFE locking. The stability based on BFE method is typically  $4.3(2) \times 10^{-12}/\sqrt{\tau}$ , which is  $5.1(4)$  dB better than that of PID locking, whose frequency stability is  $1.4(1) \times 10^{-11}/\sqrt{\tau}$ . The Dick effect limitation is estimated according to the sensitivity function and the LO phase noises.

the Heisenberg scaling ( $\Delta f_{est} \propto 1/T$ ). In further, we lock a cold-atom CPT clock with the BFE technique and yield a stability being  $5.1(4)$  dB better than that of the conventional PID locking. Benefited from the long total interrogation time offered by the BFE, our locking scheme is also suitable to lock other types of atomic clocks such as ion trap clocks, fountain clocks and optical lattice clocks.

In our experiment, the precision limit is set by the limited coherence time  $T_{max}$  of cold  $^{87}\text{Rb}$  atomic gases. Thus, the stability can be improved when long  $T_{max}$  is available, such as, cold atoms in optical lattices may have a  $T_{max}$  up to tens of seconds [57, 58]. By using our BFE protocol, the stability of an Sr optical lattice clock may [58] be improved from  $5.23 \times 10^{-17}/\sqrt{\tau}$  to  $1.16 \times 10^{-17}/\sqrt{\tau}$  with the scheme of  $\{a = 1.25, g = 1, \tilde{M} = 15, M_b = 51\}$  (see Supplementary Materials). Besides, to improve the efficiency, one can adopt

Markov-chain Monte Carlo (MMC) and particle filter method [59–61] to efficaciously reduce the amount of calculation in Bayesian updates. Furthermore, applying the BFE to many-body quantum systems [16, 62–65], the quantum projection noises can be further suppressed in the term of particle number and interrogation time simultaneously. In particular, besides the cascaded GHZ-state phase estimation [66, 67], the BFE offers another efficient method to overcome the challenge of reduced dynamic ranges in entanglement-enhanced quantum sensors [7–17, 66, 67].

### Online content

Any methods, additional references, Nature Portfolio reporting summaries, source data, extended data, supplementary information, acknowledgements, peer review information; details of author contributions and competing interests; and statements of data and code availability are available at XXX.

\* hjiahao@mail2.sysu.edu.cn

† lubo1982@szu.edu.cn

‡ chleecn@szu.edu.cn

[1] A. D. Ludlow, M. M. Boyd, J. Ye, E. Peik, and P. O.

Schmidt, Optical atomic clocks, *Rev. Mod. Phys.* **87**, 637 (2015).

[2] C. W. Chou, D. B. Hume, T. Rosenband, and D. J. Wineland, Optical clocks and relativity, *Science* **329**,

1630 (2010).

[3] V. Schkolnik, D. Budker, O. Fartmann, V. Flambaum, L. Hollberg, T. Kalaydzhyan, S. Kolkowitz, M. Krutzik, A. Ludlow, N. Newbury, C. Pyrlik, L. Sinclair, Y. Stadnik, I. Tietje, J. Ye, and J. Williams, Optical atomic clock aboard an earth-orbiting space station (OACES): enhancing searches for physics beyond the standard model in space, *Quantum Sci. Technol.* **8**, 014003 (2022).

[4] C. Sanner, N. Huntemann, R. Lange, C. Tamm, E. Peik, M. S. Safronova, and S. G. Porsev, Optical clock comparison for lorentz symmetry testing, *Nature* **567**, 204 (2019).

[5] C. J. Kennedy, E. Oelker, J. M. Robinson, T. Bothwell, D. Kedar, W. R. Milner, G. E. Marti, A. Derevianko, and J. Ye, Precision metrology meets cosmology: Improved constraints on ultralight dark matter from atom-cavity frequency comparisons, *Phys. Rev. Lett.* **125**, 201302 (2020).

[6] M. Takamoto, I. Ushijima, N. Ohmae, T. Yahagi, K. Kokado, H. Shinkai, and H. Katori, Test of general relativity by a pair of transportable optical lattice clocks, *Nat. Photon.* **14**, 411–415 (2020).

[7] J. M. Robinson, M. Miklos, Y. M. Tso, C. J. Kennedy, T. Bothwell, D. Kedar, J. K. Thompson, and J. Ye, Direct comparison of two spin-squeezed optical clock ensembles at the  $10^{-17}$  level, *Nat. Phys.* **20**, 208–213 (2024).

[8] B. C. Nichol, R. Srinivas, D. P. Nadlinger, P. Drmota, D. Main, G. Araneda, C. J. Ballance, and D. M. Lucas, An elementary quantum network of entangled optical atomic clocks, *Nature* **609**, 689–694 (2022).

[9] E. Pedrozo-Peña, S. Colombo, C. Shu, A. F. Adiyatullin, Z. Li, E. Mendez, B. Braverman, A. Kawasaki, D. Akamatsu, Y. Xiao, and V. Vuletić, Entanglement on an optical atomic-clock transition, *Nature* **588**, 414 (2020).

[10] J. Appel, P. J. Windpassinger, D. Oblak, U. B. Hoff, N. Kjærgaard, and E. S. Polzik, Mesoscopic atomic entanglement for precision measurements beyond the standard quantum limit, *PNAS* **106**, 10960 (2009).

[11] I. Kruse, K. Lange, J. Peise, B. Lücke, L. Pezzè, J. Arlt, W. Ertmer, C. Lisdat, L. Santos, A. Smerzi, and C. Klempert, Improvement of an atomic clock using squeezed vacuum, *Phys. Rev. Lett.* **117**, 143004 (2016).

[12] T. Takano, M. Fuyama, R. Namiki, and Y. Takahashi, Spin squeezing of a cold atomic ensemble with the nuclear spin of one-half, *Phys. Rev. Lett.* **102**, 033601 (2009).

[13] J. G. Bohnet, K. C. Cox, M. A. Norcia, J. M. Weiner, Z. Li, Z. Chen, and J. K. Thompson, Reduced spin measurement back-action for a phase sensitivity ten times beyond the standard quantum limit, *Nat. Photon.* **8**, 731 (2014).

[14] J. Estève, C. Gross, A. Weller, S. Giovanazzi, and M. K. Oberthaler, Squeezing and entanglement in a Bose-Einstein condensate, *Nature* **455**, 1216 (2008).

[15] O. Hosten, N. J. Engelsen, R. Krishnakumar, and M. A. Kasevich, Measurement noise 100 times lower than the quantum-projection limit using entangled atoms, *Nature* **529**, 505 (2016).

[16] L. Pezzè, A. Smerzi, M. K. Oberthaler, R. Schmied, and P. Treutlein, Quantum metrology with nonclassical states of atomic ensembles, *Rev. Mod. Phys.* **90**, 035005 (2018).

[17] J. Huang, M. Zhuang, and C. Lee, Entanglement-enhanced quantum metrology: from standard quantum limit to Heisenberg limit, *arXiv:2402.03572* (2024).

[18] R. S. Said, D. W. Berry, and J. Twamley, Nanoscale magnetometry using a single-spin system in diamond, *Phys. Rev. B* **83**, 125410 (2011).

[19] N. Wiebe and C. Granade, Efficient Bayesian phase estimation, *Phys. Rev. Lett.* **117**, 010503 (2016).

[20] B. L. Higgins, D. W. Berry, S. D. Bartlett, H. M. Wiseman, and G. J. Pryde, Entanglement-free Heisenberg-limited phase estimation, *Nature* **450**, 393 (2007).

[21] C. L. Degen, F. Reinhard, and P. Cappellaro, Quantum sensing, *Rev. Mod. Phys.* **89**, 035002 (2017).

[22] R. Santagati, A. A. Gentile, S. Knauer, S. Schmitt, S. Paesani, C. Granade, N. Wiebe, C. Osterkamp, L. P. McGuinness, J. Wang, M. G. Thompson, J. G. Rarity, F. Jelezko, and A. Laing, Magnetic-field learning using a single electronic spin in diamond with one-photon readout at room temperature, *Phys. Rev. X* **9**, 021019 (2019).

[23] R. Puebla, Y. Ban, J. Haase, M. Plenio, M. Paternostro, and J. Casanova, Versatile atomic magnetometry assisted by Bayesian inference, *Phys. Rev. Appl.* **16**, 024044 (2021).

[24] N. M. Nusran, M. U. Momeen, and M. V. Dutt, High-dynamic-range magnetometry with a single electronic spin in diamond, *Nat. Nanotechnol.* **7**, 109 (2012).

[25] C. Bonato, M. Blok, H. Dinani, D. Berry, M. Markham, D. Twitchen, and R. Hanson, Optimized quantum sensing with a single electron spin using real-time adaptive measurements, *Nat. Nanotechnol.* **11**, 247 (2016).

[26] E. D. Herbschleb, H. Kato, T. Makino, S. Yamasaki, and N. Mizuochi, Ultra-high dynamic range quantum measurement retaining its sensitivity, *Nat. Commun.* **12**, 306 (2021).

[27] X. Zheng, J. Dolde, V. Lochab, B. N. Merriman, H. Li, and S. Kolkowitz, Differential clock comparisons with a multiplexed optical lattice clock, *Nature* **602**, 425 (2022).

[28] L. Pezzè and A. Smerzi, Heisenberg-limited noisy atomic clock using a hybrid coherent and squeezed state protocol, *Phys. Rev. Lett.* **125**, 210503 (2020).

[29] H. R. Gray, R. M. Whitley, and J. Stroud, C. R., Coherent trapping of atomic populations, *Opt. Lett.* **3**, 218 (1978).

[30] M. A. Hafiz, G. Coget, M. Petersen, C. E. Calosso, S. Guérardel, E. d. Clercq, and R. Boudot, Symmetric autabalanced ramsey interrogation for high-performance coherent-population-trapping vapor-cell atomic clock, *Appl. Phys. Lett.* **112**, 244102 (2018).

[31] X. Liu, E. Ivanov, V. I. Yudin, J. Kitching, and E. A. Donley, Low-drift coherent population trapping clock based on laser-cooled atoms and high-coherence excitation fields, *Phys. Rev. Appl.* **8**, 054001 (2017).

[32] P. Yun, F. Tricot, C. E. Calosso, S. Micalizio, B. François, R. Boudot, S. Guérardel, and E. de Clercq, High-performance coherent population trapping clock with polarization modulation, *Phys. Rev. Appl.* **7**, 014018 (2017).

[33] R. Fang, C. Han, X. Jiang, Y. Qiu, Y. Guo, M. Zhao, J. Huang, B. Lu, and C. Lee, Temporal analog of Fabry-Pérot resonator via coherent population trapping, *npj Quantum Information* **7**, 143 (2021).

[34] C. Han, J. Huang, X. Jiang, R. Fang, Y. Qiu, B. Lu, and C. Lee, Adaptive Bayesian algorithm for achieving a desired magneto-sensitive transition, *Opt. Exp.* **29**, 21031 (2021).

[35] A. V. Taichenachev, V. I. Yudin, V. L. Velichansky, and S. A. Zibrov, On the unique possibility of significantly

increasing the contrast of dark resonances on the D1 line of  $^{87}\text{Rb}$ , *Jetp Lett.* **82**, 398 (2005).

[36] C. Xi, Y. Guo-Qing, W. Jin, and Z. Ming-Sheng, Coherent population trapping-Ramsey interference in cold atoms, *Chin. Phys. Lett.* **27**, 113201 (2010).

[37] E. Blanshan, S. M. Rochester, E. A. Donley, and J. Kitching, Light shifts in a pulsed cold-atom coherent-population-trapping clock, *Phys. Rev. A* **91**, 041401(R) (2015).

[38] S. V. Kargapoltev, J. Kitching, L. Hollberg, A. V. Taichenachev, V. L. Velichansky, and V. I. Yudin, High-contrast dark resonance in  $\sigma_+ - \sigma_-$  optical field, *Laser Phys. Lett.* **1**, 495 (2004).

[39] T. Zanon, S. Guerandel, E. de Clercq, D. Holleville, N. Dimarcq, and A. Clairon, High contrast Ramsey fringes with coherent-population-trapping pulses in a double Lambda atomic system, *Phys. Rev. Lett.* **94**, 193002 (2005).

[40] V. Gebhart, R. Santagati, A. A. Gentile, E. M. Gauger, D. Craig, N. Ares, L. Banchi, F. Marquardt, L. Pezzè, and C. Bonato, Learning quantum systems, *Nat. Rev. Phys.* **5**, 141 (2023).

[41] P. Cappellaro, Spin-bath narrowing with adaptive parameter estimation, *Phys. Rev. A* **85**, 030301(R) (2012).

[42] H. T. Dinani, D. W. Berry, R. Gonzalez, J. R. Maze, and C. Bonato, Bayesian estimation for quantum sensing in the absence of single-shot detection, *Phys. Rev. B* **99**, 125413 (2019).

[43] G. Waldherr, J. Beck, P. Neumann, R. S. Said, M. Nitsche, M. L. Markham, D. J. Twitchen, J. Twamley, F. Jelezko, and J. Wrachtrup, High-dynamic-range magnetometry with a single nuclear spin in diamond, *Nat. Nanotechnol.* **7**, 105 (2012).

[44] C. Ferrie, C. E. Granade, and D. G. Cory, How to best sample a periodic probability distribution, or on the accuracy of Hamiltonian finding strategies, *Quantum Inf. Process.* **12**, 611 (2013).

[45] A. Lumino, E. Polino, A. S. Rab, G. Milani, N. Spagnolo, N. Wiebe, and F. Sciarrino, Experimental phase estimation enhanced by machine learning, *Phys. Rev. Appl.* **10**, 044033 (2018).

[46] T. Ruster, H. Kaufmann, M. A. Luda, V. Kaushal, C. T. Schmiegelow, F. Schmidt-Kaler, and U. G. Poschinger, Entanglement-based dc magnetometry with separated ions, *Phys. Rev. X* **7**, 031050 (2017).

[47] W. Nagourney, J. Sandberg, and H. Dehmelt, Shelved optical electron amplifier: Observation of quantum jumps, *Phys. Rev. Lett.* **56**, 2797 (1986).

[48] R. Wynands and S. Weyers, Atomic fountain clocks, *Metrologia* **42**, S64 (2005).

[49] J.-M. Danet, M. Lours, S. Guérandel, and E. De Clercq, Dick effect in a pulsed atomic clock using coherent population trapping, *IEEE Transactions on Ultrasonics, Ferroelectrics, and Frequency Control* **61**, 567 (2014).

[50] S. M. Brewer, J.-S. Chen, A. M. Hankin, E. R. Clements, C. W. Chou, D. J. Wineland, D. B. Hume, and D. R. Leibrandt,  $^{27}\text{Al}^+$  quantum-logic clock with a systematic uncertainty below  $10^{-18}$ , *Phys. Rev. Lett.* **123**, 033201 (2019).

[51] Y. Huang, B. Zhang, M. Zeng, Y. Hao, Z. Ma, H. Zhang, H. Guan, Z. Chen, M. Wang, and K. Gao, Liquid-nitrogen-cooled  $\text{Ca}^+$  optical clock with systematic uncertainty of  $3 \times 10^{-18}$ , *Phys. Rev. Appl.* **17**, 034041 (2022).

[52] M. Takamoto, F.-L. Hong, R. Higashi, and H. Katori, An optical lattice clock, *Nature* **435**, 321–324 (2005).

[53] J. Li, X.-Y. Cui, Z.-P. Jia, D.-Q. Kong, H.-W. Yu, X.-Q. Zhu, X.-Y. Liu, D.-Z. Wang, X. Zhang, X.-Y. Huang, M.-Y. Zhu, Y.-M. Yang, Y. Hu, X.-P. Liu, X.-M. Zhai, P. Liu, X. Jiang, P. Xu, H.-N. Dai, Y.-A. Chen, and J.-W. Pan, A strontium lattice clock with both stability and uncertainty below  $5 \times 10^{-18}$ , *Metrologia* **61**, 015006 (2024).

[54] X. Lu, F. Guo, Y. Wang, Q. Xu, C. Zhou, J. Xia, W. Wu, and H. Chang, Absolute frequency measurement of the  $^{87}\text{Sr}$  optical lattice clock at ntsc using international atomic time, *Metrologia* **60**, 015008 (2023).

[55] L. Luo, H. Qiao, D. Ai, M. Zhou, S. Zhang, S. Zhang, C. Sun, Q. Qi, C. Peng, T. Jin, W. Fang, Z. Yang, T. Li, K. Liang, and X. Xu, Absolute frequency measurement of an Yb optical clock at the  $10^{-16}$  level using international atomic time, *Metrologia* **57**, 065017 (2020).

[56] Y. Lin, Q. Wang, F. Meng, S. Cao, Y. Wang, Y. Li, Z. Sun, B. Lu, T. Yang, B. Lin, A. Zhang, F. Fang, and Z. Fang, A  $^{87}\text{Sr}$  optical lattice clock with  $2.9 \times 10^{-17}$  uncertainty and its absolute frequency measurement, *Metrologia* **58**, 035010 (2021).

[57] V. Xu, M. Jaffe, C. Panda, S. Kristensen, L. Clark, and H. Müller, Probing gravity by holding atoms for 20 seconds, *Science* **366**, 745 (2019).

[58] A. Young, W. Eckner, W. Milner, D. Kedar, M. Norcia, E. Oelker, N. Schine, J. Ye, and A. Kaufman, Half-minute-scale atomic coherence and high relative stability in a tweezer clock, *Nature* **588**, 408 (2020).

[59] C. E. Granade, C. Ferrie, N. Wiebe, and D. G. Cory, Robust online Hamiltonian learning, *New J. Phys.* **14**, 103013 (2012).

[60] J. Wang, S. Paesani, R. Santagati, S. Knauer, A. A. Gentile, N. Wiebe, M. Petruzzella, J. L. O'brien, J. G. Rarity, A. Laing, and M. G. Thompson, Experimental quantum Hamiltonian learning, *Nat. Phys.* **13**, 551 (2017).

[61] Y. Qiu, M. Zhuang, J. Huang, and C. Lee, Efficient Bayesian phase estimation via entropy-based sampling, *Quantum Sci. Technol.* **7**, 035022 (2022).

[62] S. Nolan, A. Smerzi, and L. Pezzè, A machine learning approach to Bayesian parameter estimation, *npj Quantum Information* **7**, 169 (2021).

[63] J. Huang, M. Zhuang, J. Zhou, Y. Shen, and C. Lee, Quantum metrology assisted by machine learning, *Adv Quantum Technol.* , 2300329 (2024).

[64] J. Borregaard and A. S. Sørensen, Near-Heisenberg-limited atomic clocks in the presence of decoherence, *Phys. Rev. Lett.* **111**, 090801 (2013).

[65] R. Kaubruegger, D. V. Vasilyev, M. Schulte, K. Hammerer, and P. Zoller, Quantum variational optimization of Ramsey interferometry and atomic clocks, *Phys. Rev. X* **11**, 041045 (2021).

[66] A. Cao, W. J. Eckner, T. L. Yelin, A. W. Young, S. Jandura, L. Yan, K. Kim, G. Pupillo, J. Ye, N. D. Oppong, and A. M. Kaufman, Multi-qubit gates and ‘schrödinger cat’ states in an optical clock, *arXiv:2402.16289* (2024).

[67] R. Finkelstein, R. B.-S. Tsai, X. Sun, P. Scholl, S. Direkci, T. Gefen, J. Choi, A. L. Shaw, and M. Endres, Universal quantum operations and ancilla-based readout for tweezer clocks, *arXiv:2402.16220* (2024).

## Methods

## Experimental setup

The single- $\Lambda$  CPT connects the clock states  $|F = 1, m_F = 0\rangle$  and  $|F = 2, m_F = 0\rangle$  through the excited state  $|F' = 2, m_F = -1\rangle$ . A three-dimensional magnetic-optical trap (MOT) is adopted for 100 ms followed by a 5 ms molasses, which can trap and cool approximately  $10^7$   $^{87}\text{Rb}$  atoms to 20  $\mu\text{K}$ . At this moment, the atoms are fallen freely and interrogated by left-circularly polarized CPT light in a magnetic field of 35 mG. The CPT beam is generated from a laser modulated by a fiber-coupled electro-optic phase modulator (EOPM) at 6.835 GHz, which is equal to the  $^{87}\text{Rb}$  ground-state hyperfine splitting frequency. The optical carrier and positive first-order sideband are set as equal intensity and couple the clock states to the excited state. An acousto-optic modulator (AOM) is used to generate the CPT pulses. After a fiber, a Glan prism is used to purify the polarization. We use a timing diagram of a 400  $\mu\text{s}$  CPT preparation pulse  $\tau_p$  followed by an interrogation time  $T_R$  and a 50  $\mu\text{s}$  detection pulse  $\tau_d$  (Fig. 1b). The CPT beam is equally separated into two beams by a half-wave plate and a polarization beam splitter. One beam, whose polarizations are changed to  $\sigma^-$  by a quarter-wave plate, transmits through the atoms and is detected by the CPT photodetector as  $S_T$  (PD1 in Fig. 1c) while the other beam is detected by the photodetector as  $S_N$  (PD2 in Fig. 1c). The transmission signals (TSs) are given by  $S_{TS} = S_T/S_N$ , which can reduce the effect of intensity noise on the CPT-Ramsey signals.

## Basic procedure of our Bayesian frequency estimation (BFE) protocol

Our BFE protocol is implemented according to the following flowing chart, which includes,

- Step 1: Determine the values of all input parameters  $\{T_1, T_{\max}, R, a, g, \tilde{M}, M_b\}$  based on specific experimental conditions and requirements.
- Step 2: Initialize the frequency interval  $[f_l, f_r]$  and prior distribution  $p_1(f_c)$ . The frequency interval should include the clock transition frequency  $f_c$  (i.e.  $f_l < f_c < f_r$ ) and the interval width equals to the reciprocal of the minimum integration time (i.e.  $f_{lr} \equiv f_r - f_l = 1/T_1$ ). The initial prior distribution is chosen as the uniform distribution over the interval  $[f_l, f_r]$ , i.e.  $p_1(f_c) = 1/T_1^{-1}$ .
- Step 3: Implement the loop. The Ramsey time  $T_i$  is given by Eq. (4). The interval width  $f_{lr}$  is updated according to the reciprocal of the Ramsey time  $T_i$ , i.e.  $f_{lr} = 1/T_i$ . For  $i > 1$ , the frequency interval  $[f_l, f_r]$  is updated by using the previous frequency estimator  $f_{\text{est}}^{(i)}$  as the center and  $f_{lr}$  as the width, the prior distribution  $p_i(f_c)$  is reset with the estimated center  $f_{\text{est}}^{(i)}$  and the estimated standard deviation  $\Delta f_{\text{est}}^{(i)}$  given by the previous step.
- Step 4: Obtain the frequency that maximizes Eq. (5), defined as the LO frequency  $f$ .

- Step 5: Conduct experimental detection to obtain the normalized signal  $s_f$  with  $T_i$  and  $f_i$  (i.e. the population probability  $p_e$ ).
- Step 6: Perform Bayesian iteration. The likelihood function is defined by Eq. (2). The probability distribution is updated as a posterior distribution  $p(f_c|p_e; f)$  according to Bayes' formula (3). The estimated value and uncertainty of  $f_c$  can be obtained from the posterior distribution. The next update is implemented by inheriting the posterior distribution as the next prior distribution.

---

### Algorithm 1: Flowing chart of our Bayesian frequency estimation protocol

---

```

Input : minimum interrogation time  $T_1$ ;
        maximum interrogation time  $T_{\max}$ ;
        other parameters  $\{R, a, g, \tilde{M}, M_b\}$ .
Output : estimated frequency  $f_{\text{est}}$ ;
        uncertainty  $\Delta f_{\text{est}}$ .
Initialize: initial interval  $[f_l, f_r]$ ;
        initial prior distribution  $p_1(f_c) = 1/T_1^{-1}$ .
[Main Loop]:
for  $i = 1$  to  $M_b$  do
  [Updates of parameter];
  interrogation time:
     $T_{\max}/a^{(j-i)/g}$ ,  $(j-i)/g \in \mathbb{N}^+, i < j$ 
     $T_i = \begin{cases} T_{i-1}, & (j-i)/g \notin \mathbb{N}^+, i < j \\ T_{\max}, & i \geq j \end{cases}$ 
  length of interval:  $f_{lr} = 1/T_i$ ;
  if  $i > 1$  then
     $f_l \leftarrow f_{\text{est}}^{(i)} - f_{lr}/2$ ;
     $f_r \leftarrow f_{\text{est}}^{(i)} + f_{lr}/2$ ;
    reset the prior distribution
     $p_i(f_c) = \frac{1}{\sqrt{2\pi}\sigma} \exp\left[-\frac{(f_c - \mu)^2}{2\sigma^2}\right]$ , where
     $\mu = (f_l + f_r)/2$  and  $\sigma = \Delta f_{\text{est}}^{(i)}$ 
  end
  LO frequency:  $f = \arg \max_f U(f)$ 
  [Random enhancement];
  if  $T_i > T_{\max}$  then
     $| f \leftarrow f + \epsilon$ , where  $\epsilon \sim \mathcal{N}(0, 2\Delta f_{\text{est}}^{(i)})$ 
  end
  [Experimental measurement];
  frequency shift compensation:  $f \leftarrow f + f_s$ ;
  measurement normalized signal  $s_f$  using  $T_i$  and  $f_i$ ;
   $p_e \leftarrow s_f$ ;
  [Bayesian iteration];
  Likelihood function:
   $\mathcal{L}(p_e|f_c, f) = \frac{1}{\sqrt{2\pi}\sigma} \exp\left[-\frac{(p_e - \mathcal{L}_u(1|f_c, f))^2}{2\sigma^2}\right]$ , where
   $\sigma^2 = p_e(1 - p_e)/R$ ;
  Bayesian update:  $p(f_c|p_e; f) \leftarrow \mathcal{N}\mathcal{L}(p_e|f_c, f)p(f_c)$ ;
  Estimated frequency:  $f_{\text{est}} = \int f_c p(f_c|p_e; f) df_c$ ;
  Uncertainty:
   $\Delta f_{\text{est}} = \sqrt{\int f_c^2 p(f_c|p_e; f) df_c - (f_{\text{est}})^2}$ ;
end

```

---

**Data availability**

All data acquired and used in this work are available from the corresponding authors upon reasonable request.

**Code availability**

The code used in this study is available from the corresponding authors upon reasonable request.

**Acknowledgements**

C.H., Z.M. and Y.Q. contributed equally to this work. This work is supported by the National Key Research and Development Program of China (2022YFA1404104), and the National Natural Science Foundation of China (12025509, 12104521).

**Author contributions**

C.L., B.L. and J.H. conceived the project. Y.Q., J.H.

and C.L. developed the physical protocol. Y.Q. and J.H. performed the theoretical simulations. C.H., Z.M. and B.L. designed the experiment. C.H., Z.M., J.W., C.Z. and M.L. performed the experiment. All authors discussed the results and contributed to compose and revise the manuscript. C.H., Z.M. and Y.Q. contribute equally to this work. C.L. supervised the project.

**Competing interests**

The authors declare no competing interests.

**Additional information**

**Supplementary information** The online version contains supplementary material available at XXX.

**Correspondence and requests for materials** should be addressed to Jiahao Huang, Bo Lu or Chaohong Lee.